Eur. Phys. J. C (2018) 78:464
https://doi.org/10.1140/epjc/s10052-018-5803-3

THE EUROPEAN PHYSICAL JOURNAL C

Regular Article - Experimental Physics

Monte Carlo study of particle identification at the CEPC using TPC dE/dx information

F. An[1,2,a], **S. Prell**[2], **C. Chen**[2], **J. Cochran**[2], **X. Lou**[1,3,4], **M. Ruan**[1,b]

[1] Institute of High Energy Physics, Chinese Academy of Science, Beijing, China
[2] Department of Physics and Astronomy, Iowa State University, Ames, IA, USA
[3] Physics Department, University of Texas at Dallas, Richardson, TX, USA
[4] University of Chinese Academy of Science (UCAS), Beijing, China

Received: 14 March 2018 / Accepted: 12 April 2018 / Published online: 8 June 2018

Abstract The kaon identification is crucial for the flavor physics, and also benefits the flavor and charge reconstruction of the jets. We explore the particle identification capability for tracks with momenta ranging from 2–20 GeV/c using the dE/dx measurements in the Time Projection Chamber at the future Circular Electron-Positron Collider. Based on Monte Carlo simulation, we anticipate that an average 3.2 σ (2.6 σ) K/π separation can be achieved based on dE/dx information for an optimistic (conservative) extrapolation of the simulated performance to the final system. Time-of-flight (TOF) information from the Electromagnetic Calorimeter can provide K/π separation around 1 GeV/c and reduce the K/p mis-identification rate. By combining the dE/dx and TOF information, we estimate that in the optimistic scenario a kaon selection in inclusive hadronic Z decays with both the average efficiency and purity approaching 95% can be achieved.

1 Introduction

The project of building a Circular Electron-Positron Collider (CEPC) [1] in China has been proposed. The CEPC will operate as a Higgs boson factory or a Z boson factory at center-of-mass energies of $\sqrt{s} \sim 240$ or 91 GeV, respectively. During the lifetime of the CEPC, one million Higgs bosons are expected to be produced, allowing precision measurements of the Higgs boson properties [2]. In addition, ten billion Z bosons will be delivered at the Z pole promising refined measurements of electroweak and heavy flavor physics [3].

A Time Projection Chamber (TPC) has been proposed as a candidate charged particle tracking device for the CEPC detector. TPCs have been operated successfully in e^+e^- and hadron collider experiments and even in fixed-target experiments, such as the ALEPH [4] and ALICE [5] experiments at CERN, the HISS experiment at BEVALEC [6], etc. A TPC provides precise momentum and position measurements, a low material budget, and good particle identification (PID) over a wide range of momentum. The PID information is based on dE/dx measurements in the TPC, where dE/dx is defined as the energy deposit per unit path length. There are several ongoing R&D efforts about the TPC proposal, such as exploring novel technologies of the GEM-Micromegas [7] or GEM [8] readout detectors, the voxel occupancy in the TPC in decays at the Z pole [9], etc. Compared to previous TPCs, we expect an improved performance of the proposed TPC at the CEPC detector as a result of the increased number of readout channels and recent developments in readout electronics.

In this paper, the dE/dx performance of the CEPC TPC is investigated based on Monte Carlo (MC) simulation. PID will play an important role in measurements of the bottom (b) and charm (c) hadron decays in heavy flavor physics. It can also be exploited to enhance the flavor tagging of the b/c-jets in Higgs and precision electroweak measurements. We study the PID of kaons, pions and protons in hadronic decays at the Z pole, demonstrating that an effective kaon selection can be achieved by combining the dE/dx measurements of the TPC with the time-of-flight (TOF) information provided by the Electromagnetic Calorimeter (ECAL) at the CEPC detector.

The paper is organized as follows. In Sect. 2 we present the configuration of the CEPC TPC and the energy loss measurement of traversing charged particles. Section 3 describes the key factors influencing the resolution of the dE/dx measurement and provides an estimate of the PID performance at the CEPC. In Sect. 4 a brief conclusion is given.

[a] e-mail: anff@ihep.ac.cn
[b] e-mail: manqi.ruan@ihep.ac.cn

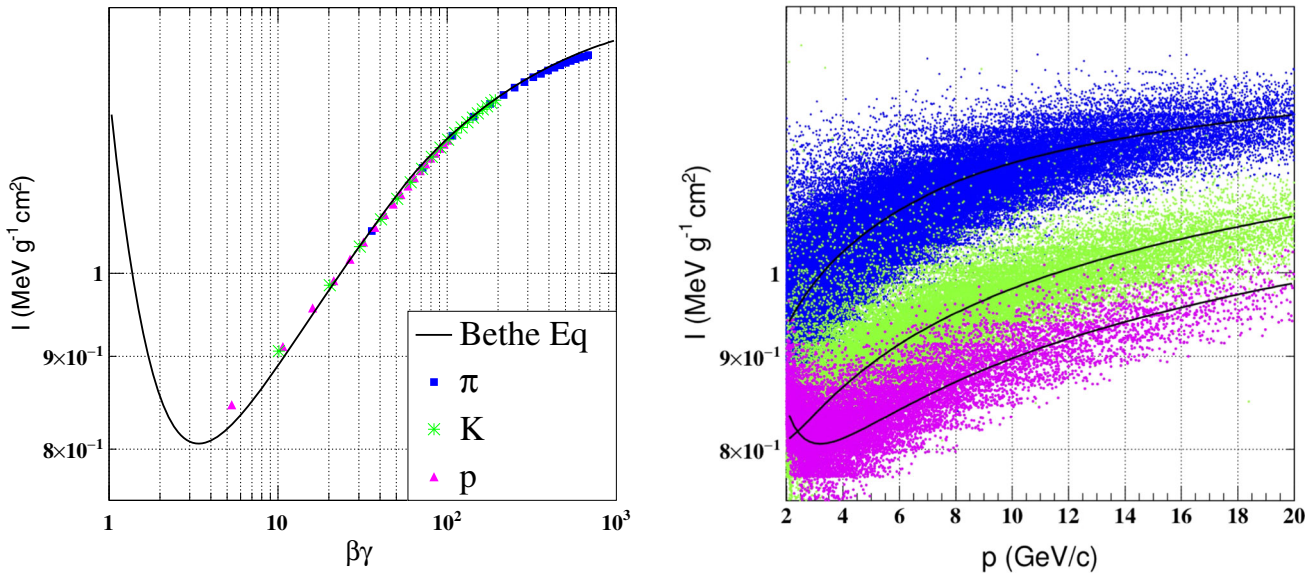

Fig. 1 The dependence of the truncated mean I of the track dE/dx, as a function of $\beta\gamma$ (left) and p (right) for charged particles traversing the TPC of the CEPC detector. In the left plot the dots represent the MC result of single-particle events with the theoretical prediction by the Bethe equation [16] overlaid. In the right plot the dots are from simulation of $e^+e^- \to Z \to q\bar{q}$ events

2 Energy deposit in TPC

The TPC concept was introduced in Refs. [10,11]. A TPC consists essentially of a wireless drift volume situated between parallel axial electric and magnetic fields, where the electric field is set up between a central cathode plate and the end plates. When a charged particle traverses the gas-filled drift volume, it generates electron-ion pairs by collisions with the gas molecules. The electrons drift towards the end plates, where the charges are amplified and collected.

The default design of the TPC at the CEPC detector can be found in Ref. [1]. It is a cylindrical detector that is 4.7 m long with an inner and outer radii of 0.325 and 1.8 m, respectively. The candidate gas is an argon-based gas composite (93% Ar + 5% CH_4 + 2%CO_2) held at atmospheric pressure and room temperature. A solenoid provides a magnetic field of 3 T along the beam direction. In the endcaps, Micromegas [12] detector modules with pad size of 6 mm along the radial direction (height) and 1 mm along the azimuthal direction (width) are arranged in 222 concentrical rings.

In the MC simulation, the description of the detector geometry, material and the ionization process are implemented using GEANT4 [13]. Single-particle events are generated using ParticleGun. Collision events of the Standard Model processes are produced with the event generator WHIZARD [14]. The dE/dx measurement by each pad is defined as the energy deposit divided by the track length in the corresponding drift volume, both of which are provided by GEANT4. Typically, the dE/dx measurements of a track follow a Landau distribution with a large tail caused by high-energy δ-electrons. We estimate a representative average dE/dx for a track, denoted as I, by using the common "truncated mean" method [15]. We calculate I as the mean of the lowest 90% of the dE/dx values associated with the track, where the truncation ratio of 90% is determined to yield the optimal dE/dx resolution. The distribution of the truncated mean I can be well described by a Gaussian function with a width denoted as σ_I. Unless explicitly stated, the dE/dx resolution in the paper refers to the ratio σ_I/I.

For a particle with momentum p and mass m, the MC simulation of the dependence of I as a function of $\beta\gamma = p/(mc)$ is shown in the left plot of Fig. 1. Herein we use single-particle events requiring $\theta = 45°$ so that the tracks traverse the full TPC radius, where θ is defined as the polar angle of the tracks with respect to the beam direction. The simulated I dependence agrees well with the theoretical prediction by the Bethe equation [16]. The values of all the parameters in the Bethe equation are taken from Ref. [17] except for the normalization scale factor and the maximum energy transfer $W_{\max}$, which is free in the fit to the I distribution following the procedure in Ref. [18]. In the right plot of Fig. 1, the scatter plot of I versus p is presented using a simulated sample of $e^+e^- \to Z \to q\bar{q}$ events. At the CEPC, the majority of the particles traversing the TPC have a momentum above 1 GeV/c and reside in the relativistic rise region, where TOF measurements can not effectively distinguish between the different particles types. Therefore, improving the dE/dx resolution will directly benefit the PID performance.

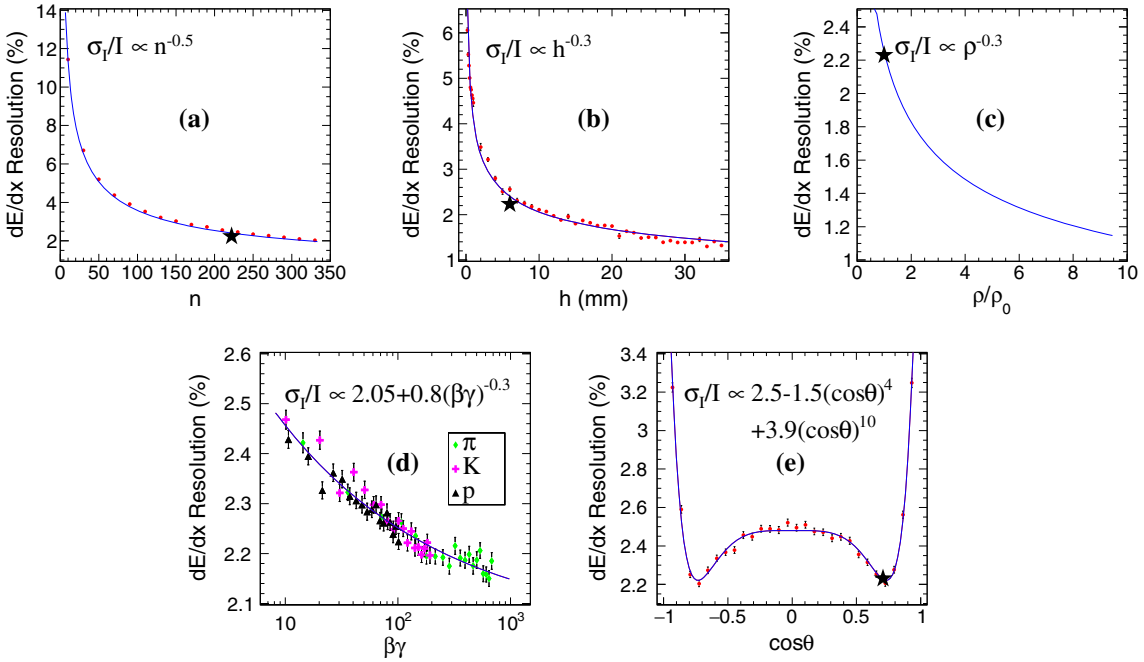

Fig. 2 The intrinsic dE/dx resolution versus the number of pad rings (**a**), the pad height along the radial direction (**b**), the ratio of gas density ρ over the default gas density ρ_0 (equivalent to the ratio of corresponding pressures) (**c**), the relativistic velocity $\beta\gamma$ (**d**) and $\cos\theta$ (**e**) of the ionizing particle. The default working point is indicated with a solid star symbol. Solid lines represent the fit projections

3 Resolution of energy deposit in TPC

In an ideal case, the dE/dx resolution for a given track depends on the number of the dE/dx measurements along the particle trajectory and the number of the ionizing electrons per measurement. We name the induced resolution from these factors "intrinsic dE/dx resolution". The resolution in real experiments, named as "actual dE/dx resolution", will be deteriorated by the detector effects arising in the processes of electron drift, signal amplification and readout in TPC. A detailed study of those effects is beyond the scope of the paper. In this paper, we study the intrinsic dE/dx resolution of the CEPC TPC using MC simulation, and estimate the degradation of the actual resolution by comparing the MC-based results with the experimental measurements of previous TPCs.

3.1 Parameterization of the intrinsic dE/dx resolution

The intrinsic dE/dx resolution arises from fluctuations at the primary ionization stage. It depends on the number of the pad rings n, the pad height along the radial direction h, the density of the working gas ρ, the relativistic velocity $\beta\gamma$ and the polar angle θ of the particle trajectory. The resolution dependence on these variables is studied using single-particle MC events. We scan each variable to obtain its relationship with the intrinsic resolution. Except for the variable under consideration, all others are kept constant at their default values given in Sect. 2, i.e., $n = 222$, $h = 6$ mm, $\rho = \rho_0 = 1.73$ mg/cm^3 and $\theta = 45°$ for pions with a momentum of 20 GeV/c. The MC results are shown in Fig. 2.

The correlations between the variables are small. To a good approximation, the parameterization of σ_I/I can be factorized as

$$\frac{\sigma_I}{I} = \frac{13.5}{n^{0.5}\cdot(h\rho)^{0.3}}[2.05 + 0.8(\beta\gamma)^{-0.3}] \times [2.5 - 1.5(\cos\theta)^4 + 3.9(\cos\theta)^{10}], \quad (1)$$

where h and ρ are in of mm and mg/cm^3, respectively. To check the correlation between the variables, we validate the factorization in the five-dimensional space by varying the variables within the ranges shown in Fig. 2. In addition, the influence of the magnetic field is found to be negligible on the dE/dx resolution. When the magnetic field is set to zero, the induced relative change of σ_I/I is within 3% for particles with momenta larger than 1 GeV/c. We also vary the truncation ratio from 60–95% and observe a 10% resolution improvement at the optimal 90% point compared to the worst case of 60% truncation.

As Eq. (1) is derived from single-particle events, its applicability to physics events is validated using kaons from $e^+e^- \to Z \to q\bar{q}$ MC events. The kinematic distributions are shown in Fig. 3. We integrate Eq. (1) over the $\cos\theta$ dis-

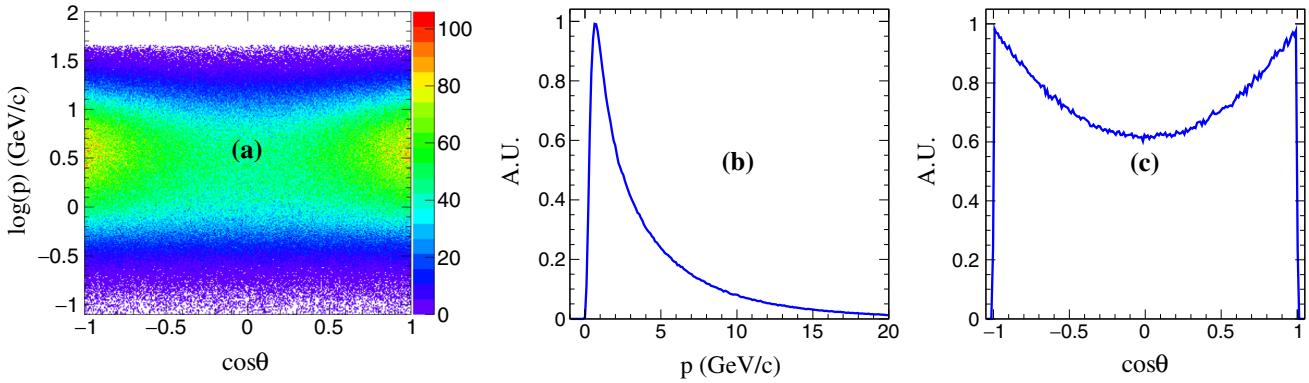

Fig. 3 Kinematic distribution of kaons in $e^+e^- \to Z \to q\bar{q}$ MC events as a function of $\log(p)$ and $\cos\theta$ (**a**), p (**b**), and $\cos\theta$ (**c**)

tribution given in Fig. 3 and calculate the average dE/dx resolution versus $\beta\gamma$. It is found to be consistent with the one directly obtained from MC. For example, for kaons with a momentum of 5 GeV/c in hadronic decays at the Z pole, the intrinsic dE/dx resolution is 3.1%.

3.2 Expected actual dE/dx resolution of the CEPC TPC

In real experiments, both detector effects and imperfect calibration can deteriorate the dE/dx resolution. We estimate the potential degradation in previous TPCs by comparing their experimental achievements with the corresponding intrinsic dE/dx resolutions obtained from MC simulation.

The TPCs considered in this study are summarized in Table 1. The information about the experiments, unless explicitly stated, is taken from the references listed in the first row. All the factors influencing the intrinsic resolution are implemented in MC simulation, including the composition of the working gas, the geometry of the TPC, the control samples and the truncation ratio used to remove the Landau tail. In the MC study, we resort to single-particle events and make them have identical particle type and kinematic distributions with the corresponding control samples used in the experiments. For the case where minimum ionizing pions are used, we assume a flat $\cos\theta$ distribution in the simulation when their $\cos\theta$ spectrum is not provided in the references. The relative uncertainty arising from such an approximation is estimated to be within a few percent and can be neglected.

Besides the factors discussed above, the number of the effective hits used for the dE/dx calculation, denoted as N_{eff}, is also considered because it greatly influences the dE/dx resolution in the earlier experiments. In TOPAZ and DELPHI, for example, on average only 60–70% effective TPC hits are available for tracks in jets due to the large size of their TPC readouts and resulting in serious hit overlap. STAR and ALICE have made significant progress in exploiting high-granularity readouts to handle their dense tracking environment. In ALICE, the fraction of N_{eff} is about 93% or even larger in proton-proton collisions [30]. Compared to ALICE, the CEPC TPC will have a higher granularity and endure much smaller track multiplicities. Therefore we neglect this effect at the CEPC. Even if assuming that 5% of the hits are discarded, the resulting relative change in the dE/dx resolution is within 3% according to Eq. (1).

In the last row of Table 1, the relative difference between the intrinsic and actual dE/dx resolutions are listed. It varies from 0.15 to 0.50 between the different experiments. Studies performed by the ALICE TPC Collaboration [31,32] show that the main detector effects causing the deterioration include diffusion in the drift volume, fluctuations in the amplification and DAQ processes, and cross talk between the readout pads. Based on MC simulation, we estimate that these effects will cause a degradation of at least 20% at the CEPC TPC. Therefore, we define two scenarios for further discussion about the dE/dx performance that might eventually be achieved by the CEPC, namely an "optimistic scenario" and a "conservative scenario", corresponding to degradations of 20 and 50%, respectively, with respect to the intrinsic dE/dx resolution.

3.3 Expected PID performance of the CEPC TPC

A common figure of merit for the PID performance is the separation power S. Between particle types A and B we define

$$S_{AB} = \frac{|I_A - I_B|}{\sqrt{\sigma_{I_A}^2 + \sigma_{I_B}^2}}, \tag{2}$$

where I_A (I_B) and σ_{I_A} (σ_{I_B}) are the average dE/dx measurement of particle type A (B) and the corresponding resolution. In the ideal case assuming no degradation and σ_I follows Eq. (1), we estimate $S_{K\pi}$ at the CEPC as a function of p and $\cos\theta$ (see Fig. 4).

One often cares about the average separation power $\langle S \rangle$ versus momentum after integrating over the $\cos\theta$ dimension. Given the $\cos\theta$ distribution in $e^+e^- \to Z \to q\bar{q}$ decays

Table 1 Properties of TPCs in previous experiments. Comparison of the relative dE/dx resolution between MC and experimental measurements

Experiment	PEP-4 [19–21]	TOPAZ [22,23]	DELPHI [24–26]	ALEPH [4,27]	STAR [28,29]	ALICE [5,30]	CEPC
Start of data taking	1982	1987	1989	1989	2000	2009	–
Colliding Particles	e^-/e^+	e^-/e^+	e^-/e^+	e^-/e^+	Au/Au	p/p	e^-/e^+
E_{beam} (GeV)	14.5	26	45.6	45.6	100	1380	125
	Ar: 0.8	Ar: 0.9	Ar: 0.8	Ar: 0.91	Ar: 0.9	Ne: 0.857	Ar: 0.93
Gas	CH_4: 0.2	CH_4: 0.1	CH_4: 0.2	CH_4: 0.09	CH_4: 0.1	CO_2: 0.095	CH_4: 0.05
						N_2: 0.048	CO_2: 0.02
Pressure (atm)	8.5	3.5	1	1	1	1	1
ρ (mg/ml)	12.43	5.47	1.46	1.57	1.56	0.95	1.73
n	183	175	192	344	13, 32[c]	63, 64, 32[c]	222
h (mm)	4	4	4	4	12, 20[c]	7.5, 10, 15[c]	6
Length (mm)	2000	3000	2680	4400	4200	5000	4700
Control Sample	e	π	π	e	π	π	K
p (GeV/c)	14.5	0.4–0.6	0.4–0.6	45.6	0.4–0.6	6.0	5.0
Truncation range	0–65%	0–65%	8–80%	8–60%	0–70%	0–60%	0–90%
N_{eff}	n	$0.7n$[a]	$0.6n$[b]	338	44	149	n
$(\sigma_I/I)_{\text{MC}}$	2.6%	3.8%	5.4%	3.0%	5.3%	3.3%	3.1%
$(\sigma_I/I)_{\text{exp}}$	3.5%	4.6%	6.2%	4.4%	6.8%[d]	5.0%	–
$\left\lvert\frac{(\sigma_I/I)_{\text{exp}}}{(\sigma_I/I)_{\text{MC}}}-1\right\rvert$	0.35	0.21	0.15	0.47	0.28	0.52	–

[a]It's required that at least 78 hits are used for the dE/dx calculation [23]. Here we assume there are 70% effective hits.
[b]65% tracks have more than 40 isolated hits, and 35% more than 100 [24]. We assume there are 60% effective hits.
[c]In the STAR and ALICE detectors, the inner, intermediate and outer subdetectors have different pad sizes.
[d]See Fig. 21 in Ref. [29]

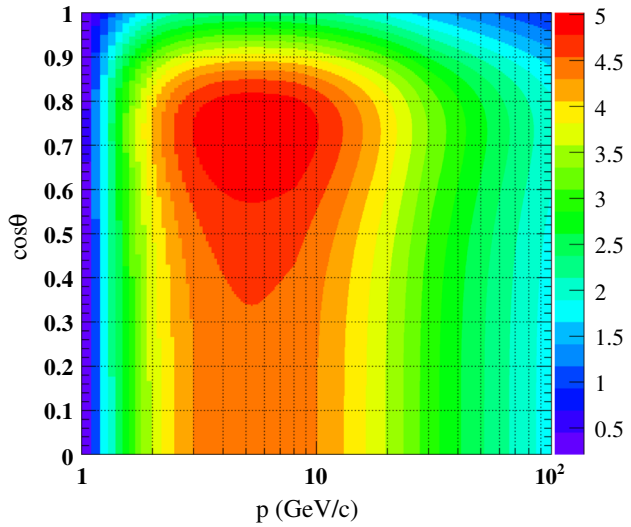

Fig. 4 Separation power $S_{K\pi}$ between kaons and pions in the p-cos θ plane using dE/dx measurements of the CEPC TPC for the ideal simulation

(see Fig. 3), the plots of $\langle S_{K\pi}\rangle$ and $\langle S_{Kp}\rangle$ as a function of p are shown in Fig. 5. In the left plot, the separation powers using dE/dx for different TPC performance scenarios are illustrated. One can see that dE/dx alone is incapable of K/π separation around 1 GeV/c and yields poor K/p separation beyond 1.5 GeV/c. To overcome this disadvantage, the exploitation of TOF information is considered.

According to a recent study on the CMS high-granularity calorimeter [33], precise TOF information could be provided by the CEPC ECAL with a precision of tens of picoseconds. Supposing TOF information with a 50 ps time resolution, and given the dE/dx measurements in the conservative scenario, the average K/π and K/p separation powers are calculated using both dE/dx and TOF. They are shown in the middle and right plots of Fig. 5. Accounting for the time resolution and the location of the ECAL, the TOF information can provide K/π (K/p) separation better than 2.5 σ up to 2.1 (4.0) GeV/c. By combining TOF and dE/dx, more than 2.0 (1.4) σ K/π (K/p) separation can be achieved up to 20 GeV/c.

The PID performance depends on the kinematic distributions and relative abundance of the charged particles in the sample under study. As an example, we take the process $e^+e^- \to Z \to q\bar{q}$ (see Fig. 3) with an average of 20 charged particles per event, of which 85% are pions, 10% are kaons, and 4% are protons. We calculate the average separation powers $\langle S_{K\pi}\rangle$ and $\langle S_{Kp}\rangle$ for particles with momenta in the range from 2–20 GeV/c. They are listed in Table 2. Particles with momenta smaller than 2 GeV/c are not considered since they can be clearly separated.

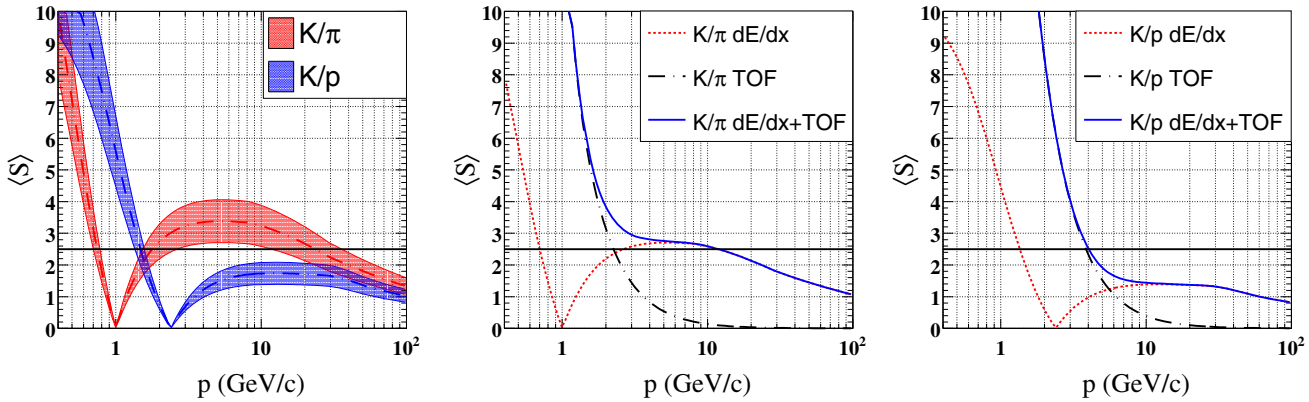

Fig. 5 Average separation power $\langle S \rangle$ versus momentum between different particle types in hadronic decays at the Z pole. Left: only dE/dx is used. The bands delimit the area between the ideal simulation and the conservative scenario for the CEPC TPC. The optimistic scenario is shown as dash-dotted lines. Middle and right: dE/dx (in the conservative scenario) and/or TOF are used for K/π and K/p separation. The black solid line corresponds to 2.5 σ separation

Due to the importance of the kaon selection performance for flavor physics, we also provide an estimation of the kaon selection efficiency ε_K and the corresponding purity p_K, together with the probability of mis-identifying pions (protons) as kaons $p_{\pi(p)\to K}$. They are defined as

$$\begin{aligned} \varepsilon_K &= \frac{N_{K\to K}}{N_K}, \\ p_K &= \frac{N_{K\to K}}{N_{K\to K} + N_{\pi\to K} + N_{p\to K}}, \\ p_{\pi\to K} &= \frac{N_{\pi\to K}}{N_\pi}, \\ p_{p\to K} &= \frac{N_{p\to K}}{N_p}, \end{aligned} \tag{3}$$

where N_K, N_π, N_p are the total numbers of generated kaons, pions and protons that traverse the innermost pad ring of the TPC, $N_{K\to K}$ is the number of correctly identified kaons, and $N_{\pi(p)\to K}$ is the number of pions (protons) mistakenly identified as kaons.

The kaon selection is performed based on the variable $(I - I_K)/\sigma_I$, where I and I_K are the experimental measurement (either by dE/dx alone or by combining dE/dx and TOF) and the expected value for the kaon hypothesis respectively, and σ_I denotes the experimental resolution. Their spectra should be close to Gaussian distributions with a width of 1. In Fig. 6 we illustrate the scaled spectra of kaons, pions and protons with a momentum of 5 GeV/c using dE/dx alone assuming a 20% degradation. According to Eq. (2), the peaks between the kaon and pion (proton) spectra should be $\sqrt{2}S_{K\pi}$ ($\sqrt{2}S_{Kp}$) apart, where $S_{K\pi}$ (S_{Kp}) is the corresponding separation power. The relative populations N_π/N_K and N_K/N_p vary versus momentum and are determined based on MC simulation. We choose the intersections of the spectra as the cut points (marked by the arrows in the plot), in order to calculate the kaon identification efficiency and purity together with the mis-identification rates according to Eq. (3). We calculate these parameters at each momentum point from 2–20 GeV/c in $e^+e^- \to Z \to q\bar{q}$ events (see Fig. 3) and provide in Table 2 the average values. The MC sample under study is large enough ($\sim$ 8 million) and the statistical errors are negligibly less than 0.1%.

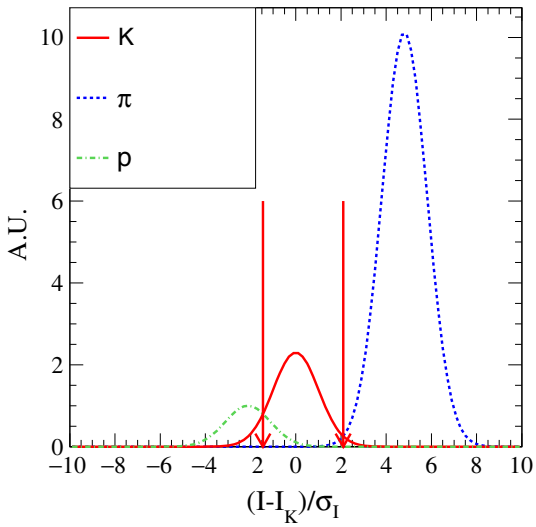

Fig. 6 The scaled spectra of $(I - I_K)/\sigma_I$ using dE/dx measurements alone for particles with a momentum of 5 GeV/c, assuming a 20% degradation. The relative populations are $N_\pi = 4.4N_K$ and $N_K = 2.3N_p$ according to MC simulation. The intersections marked by the arrows are chosen as the cut points

In the ideal simulation, the dE/dx measurements ultimately provide roughly 4 σ (1.5 σ) separation between kaon and pion (proton) in inclusive $e^+e^- \to Z \to q\bar{q}$ decays. The overall kaon identification efficiency reaches 93.2% with a

Table 2 Expected PID performance parameters at the CEPC in different scenarios. Shown are the average value of particles with momenta from 2–20 GeV/c in the $e^+e^- \to Z \to q\bar{q}$ decays

	Deterioration	0	0.5	0.2
	$\langle S_{K\pi} \rangle$	3.9	2.6	3.2
	$\langle S_{Kp} \rangle$	1.5	1.0	1.2
dE/dx	ε_K (%)	93.2	84.5	90.9
	p_K (%)	86.5	76.1	82.4
	$p_{\pi \to K}$ (%)	0.1	1.3	0.5
	$p_{p \to K}$ (%)	33.0	47.2	40.1
	$\langle S_{K\pi} \rangle$	4.0	2.8	3.4
dE/dx	$\langle S_{Kp} \rangle$	3.2	2.8	3.0
&	ε_K (%)	96.8	90.4	95.0
TOF	p_K (%)	97.0	90.1	94.5
	$p_{\pi \to K}$ (%)	0.1	1.1	0.4
	$p_{p \to K}$ (%)	6.4	13.8.	9.6

purity of 86.5%. The PID performance is limited by the proton contamination. By combining the dE/dx and TOF measurements, the K/p separation is greatly enhanced from 1.5 σ to 3.2 σ. As a consequence, the kaon identification efficiency is improved to 96.8% with a corresponding purity of 97.0%

In the conservative scenario, the kaon identification efficiency and purity degrade significantly mainly due to the more serious proton contamination. In this case, the TOF measurement plays a crucial role and can ameliorate the performance back to an efficiency of 90.4% and a purity of 90.1%. If the optimistic scenario can be realized at the CEPC, by combining dE/dx and TOF, we expect the efficiency reaches 95.0% for kaon identification with a purity of 94.5%, which is only slightly degraded from the ideal simulation. In all scenarios, the pion mis-identification rate can be controlled at a 1% level.

4 Conclusion

Effective particle identification will enrich the CEPC physics program, especially when operating at the Z pole. Using a GEANT4-based MC simulation, we study the PID performance at the CEPC based on the dE/dx measurements in the TPC and the TOF information provided by the ECAL with an assumption of 50 ps time resolution.

We explore the kaon identification performance in the momentum range from 2–20 GeV/c in inclusive hadronic Z decays, showing that an effective kaon identification can be achieved with the combined information of dE/dx and TOF. If the degradation of the dE/dx measurements due to detector effects can be controlled to less than 20%, both the average kaon identification efficiency and purity can approach 95%.

More detailed microscopic simulation and beam tests are expected to validate these conclusions in the future.

Acknowledgements We thank Keisuke Fujii, Roman Poeschl and Francois Richard for their enlightening discussion, and the continuous R&D efforts of the LCTPC collaboration. We would also express our great appreciation to Prof. Peter Christiansen of Lund University for his very helpful suggestions, especially towards the technical questions and estimations.
This work was supported by National Key Program for S&T Research and Development under Contract number 2016YFA0400400; the Hundred Talent programs of Chinese Academy of Science under Contract number Y3515540U1; National Natural Science Foundation of China under Contract number 11675202; IHEP Innovation Grant under Contract number Y4545170Y2; Chinese Academy of Science Focused Science Grant under Contract number QYZDY-SSW-SLH002; Chinese Academy of Science Special Grant for Large Scientific Project under Contract number 113111KYSB20170005; National 1000 Talents Program of China.

References

1. M. Ahmad et al., CEPC-SPPC Pre-CDR. Chap. **6**, 163 (2015)
2. M. Ruan, Nucl. Part. Phys. Proc. **273**, 857 (2016)
3. J. Fan et al., JHEP **09**, 196 (2015)
4. W.B. Atwood et al., Nucl. Instrum. Methods A **306**, 446–458 (1991)
5. J. Alme et al., Nucl. Instrum. Methods A **622**, 316–367 (2010)
6. G. Rai et al., The HISS TPC, LBL–27620 (1989)
7. Y. Zhang et al., Chin. Phys. C **38**(4), 046001 (2014)
8. D. Attie et al., Nucl. Instrum. Methods **A856**, 109 (2017)
9. M. Zhao et al., arXiv:1704.04401 [hep-ex]
10. D. Nygren, The Time Projection Chamber, PEP–198 (1975)
11. D. Nygren, Proposal for a PEP facility based on the TPC, PEP4-December 30 (1976)
12. Y. Giomataris et al., Nucl. Instrum. Methods A **376**, 29 (1996)
13. S. Agostinelli et al., GEANT4 Collaboration, Nucl. Instrum. Methods Phys. Res. Sect. A **506**, 250 (2003)
14. W. Kilian, T. Ohl, J. Reuter, Eur. Phys. J. C **71**, 1742 (2011)
15. D. Jeanne et al., Nucl. Instrum. Methods **111**, 287 (1973)
16. C. Patrignani et al., Particle Data Group, Chin. Phys. C **40**, 100001, 442 (2016)
17. R.M. Sternheimer, M.J. Berger, S.M. Seltzer, At. Data Nucl. Data Tables **30**, 261 (1984)
18. J. Va'Vra, Nucl. Instrum. Methods **A453**, 262 (2000)
19. R.J. Madaras et al., *LBL-17806, C84-03-04 Proceeding*, pp. 413–444
20. G.R. Lynch, N.J. Hadley, *Proceedings of the International Conference on Instrumentation for Colliding Beam Physics* (1982)
21. A. Barbaro-Galtieri, *Proceedings of the International Conference on Instrumentation for Colliding Beam Physics* (1982)
22. T. Kamae et al., Nucl. Instrum. Methods A **252**, 423–430 (1986)
23. A. Shirahashi et al., IEEE **35**, 414 (1988)
24. Y. Sacquin, Nucl. Instrum. Methods A **323**, 209–212 (1992)
25. P. Abreu et al., Nucl. Instrum. Methods A **378**, 57–100 (1996)
26. C. Brand et al., IEEE **36**(1), 122 (1989)

27. D. Buskulic et al., Nucl. Instrum. Methods A **360**, 481–506 (1995)
28. M. Anderson et al., Nucl. Instrum. Methods A **499**, 659–678 (2003)
29. H. Bichsel, Nucl. Instrum. Methods A **562**, 154–197 (2006)
30. J. Adam et al., Phys. Rev. C **93**, 034913 (2016)
31. D. Antonczyk et al., ALICE TPC Collaboration, Nucl. Instrum. Methods A **565**, 551 (2006)
32. P. Christiansen et al., ALICE TPC Collaboration, Nucl. Instrum. Methods A **609**, 149 (2009)
33. D. del Re, J. Phys. Conf. Ser. **587**, 012003 (2015)